Supplemental Online Material for:

The 2005 Study of Organic Aerosols at Riverside (SOAR-1): Instrumental Intercomparisons and Fine Particle Composition

Kenneth S. Docherty[1,2,*] , Allison C. Aiken[1,2,**], J. Alex. Huffman[1,2,***], Ingrid M. Ulbrich[1,2], Peter F. DeCarlo[1,3,****], Donna Sueper[1,2,4], Douglas R. Worsnop[4], David C. Snyder[5,*****], Richard E. Peltier[6,******], Rodney J. Weber[6], Brett D. Grover[7], Delbert J. Eatough[7], Brent J. Williams[8,*******], Allen H. Goldstein[8], Paul J. Ziemann[9], and Jose L. Jimenez[1,2,*]

Comparison of AMS-PMF and TD-AMS-PMF analyses

The composition of NR-PM_1 OA measured during SOAR-1 was investigated using positive matrix factorization (PMF). Separate analyses were conducted both in the absence (AMS-PMF) and presence (TD-AMS-PMF) of thermally-denuded measurements (ref. discussion in main text) and solutions containing one through twelve factors were investigated in detail. The PMF fit parameter (Q) reflects the degree to which variability in OA concentrations and mass spectra is explained by the particular solution and its minimization has been proposed as a primary criterion to determine the appropriate number of factors in a PMF solution . In this case, however, Q can also be used generally to indicate whether the AMS-PMF or TD-AMS-PMF analysis more successfully explains variability in SOAR-1 OA data. Normalized Q values (i.e., Q/Q_{exp}) obtained from both analyses are shown in Fig. S1a as a function of the number of factors included therein.

In an ideal case, Q/Q_{exp} should approach unity . In the analysis of real datasets, however, Q/Q_{exp} values are larger. Throughout the range of solutions investigated, Q/Q_{exp} values from both AMS-PMF and TD-AMS-PMF analyses steadily decrease as the number of factors is increased. In general, however, Q/Q_{exp} obtained from TD-AMS-PMF solutions are considerably (~30%) lower than those from AMS-PMF solutions indicating that the TD-AMS-PMF analysis accounts for considerably more of the variability in OA composition. This general trend is also observed when Q/Q_{exp} values within a particular solution are plotted versus FPeak. Fig. S1b shows the value of

Q/Q_{exp} as a function of FPeak for the AMS-PMF and TD-AMS-PMF 8-factor solutions where minimum Q/Q_{exp} values are observed for FPeak=0. Correlations of factor mass spectra with those of applicable standards and factor time series with those of external tracers (ref. discussion in text) did not improve for non-zero FPeak values. As a result, AMS-PMF and TD-AMS-PMF solutions with FPeak=0 were selected for more detailed comparison.

Fig. S2a and S2b show the relative contributions of factors resolved in both the TD-AMS-PMF and AMS-PMF 2- to 11- factor solutions, respectively, to total OA. Mass spectra of available standards and time series of available tracers have been used to attribute each factor to a corresponding OA component and the number of components identified in each solution are noted in parentheses at the bottom of Fig. S2a and Fig. S2b. Note that in the case of the 5- to 11- factor solutions, several resolved factors were combined to form a single OA component. In each case, the OA component resulting from this combination had a mass spectrum and temporal behavior (e.g., high correlation with NR-PM1 SO4) highly similar to that of the previously-identified low-volatility oxidized organic aerosol (LV-OOA) component . In this case, we refer to this component as composite LV-OOA (cLV-OOA) due to its origins through compiling multiple factors.

In general, the majority of solutions from both AMS-PMF and TD-AMS-PMF analyses are generally similar in terms of both the number and relative contribution of identified components to total OA although some small differences exist between these analyses. For example, for solutions containing less than eight factors, AMS-PMF

solutions fail to resolve the local OA component LOA-2, which is identified in the 6-factor TD-AMS-PMF solution. Also, in solutions containing more than eight factors, the AMS-PMF solution resolves only a single MV-OOA component while the TD-AMS-PMF solution resolves this component into two distinct subcomponents with widely differing volatility and mass spectra. Note that the 12-factor solution in each analysis (not shown) is essentially identical to the 11-factor solution. Within this range, only the 8-factor solution from each analysis was found to provide similar results both in terms of the components identified and their relative contribution to OA. These solutions are essentially equivalent. Components identified from the both 8-factor solutions include HOA, two LOA components, and several OOA components including cLV-OOA, MV-OOA, and SV-OOA.

The degree of similarity among time series and mass spectra of the various components resolved in the 8-factor AMS-PMF and TD-AMS-PMF solutions are evaluated by the correlation plots shown in Fig. S3. In these figures, the correlation between component time series (r^{TS}) is plotted against the corresponding correlation between component mass spectra (r^{MS}). In general, data points closer to the origin are more different while those further from the origin are more similar. Correlation plots for the AMS-PMF solution are shown in Fig. S3a while those for the TD-AMS-PMF solution are shown in Fig. S3b. In general, the bulk of data points in the TD-AMS-PMF solution lie closer to the origin indicating that the various components obtained from this solution are more completely resolved. This is particularly true among the identified OOA components cLV-OOA and SV-OOA. As shown in Fig. S3a, mass spectra of the cLV-

OOA and SV-OOA are highly correlated while the time series of these components are inversely correlated (r^{MS}=0.99, r^{TS}=-0.66). The correlation between the mass spectra of these components decreases slightly in the TD-AMS-PMF solution (r^{MS}=0.74) while there is essentially no correlation between their time series. Overall, the same is generally true for the remaining OOA components as well although somewhat less dramatic.

AMS-PMF and TD-AMS-PMF solutions are more directly compared in Fig. S3c wherein r^{MS} between corresponding components is plotted against complementary r^{TS} values. Here again, r^{MS} and r^{TS} values far from the origin indicate a high degree of similarity between corresponding components while values closer to the origin indicate the opposite. Note that the r^{MS} axis has been expanded for clarity due to the similarity between the mass spectra of components identified in each solution. As this plot shows, the majority of components identified in both solutions are strongly correlated with the exception of cLV-OOA and SV-OOAwhich are strongly anti-correlated in time. This large degree of correlation is largely eliminated, however, when cLV-OOA and SV-OOA are combined in a process similar to that used in the creation of cLV-OOA.

Collectively, Fig. S3 shows that there is abundant contrast among the mass spectra and time series of HOA and LOA factors. Although the resolution of these components appears to be similar to or perhaps slightly better in the TD-AMS-PMF analysis (as evidenced by smaller correlation values in Fig. S3a and S3b), both solutions effectively resolve these components. Mass spectra of the various OOA components, however, are highly similar and are much more difficult for PMF to resolve

as a result . TD-AMS-PMF analysis, however, appears to improve the resolution of various OOA components, however, as evidenced by the lower degree of correlation between OOA time series and mass spectra.

Due to rapid mode switching and temperature cycling of the TD, the interface of the TD with the HR-AMS (TD-AMS) not only provides chemically-resolved measurements of NR-PM_1 component volatility, but also introduces more variance into OA composition over time relative to routine ambient sampling. Under ambient conditions, the composition of OA is influenced by a number of factors including transport due to changing air flow patterns, strong photochemistry, and changing source contributions among others. This change, however, is affected throughout the day and proceeds over the course of a few hours. In addition, absent a dramatic change in environmental conditions, changes in OA composition can by relatively minor over the course of several hours which is disadvantageous to optimal PMF outputs. In contrast, in the case of the TD-AMS, OA composition changes as more volatile OA components are removed from the particle when TD temperature is increased and visa versa and due to sample mode cycling this change is repeated frequently, thereby introducing additional contrast among OA components which is critical to the success of PMF. Such increases in OA spectral variance under routine sampling conditions (e.g., via wide variance in ambient temperature) has been found to improve the resolution among OOA components . It is reasonable, therefore, that the analysis of TD-AMS data leads to improved resolution among the various OA, including OOA, components. An additional benefit of this type of analysis, as discussed in is the provision of information

regarding the relative volatility of various OA components. The introduction of a volatility dimension into PMF analyses expands the number of criteria which PMF users can employ to determine the unique nature of resolved factors.

Results of comparing AMS-PMF and TD-AMS-PMF analyses during SOAR-1 indicate that each provides generally similar information regarding the composition of OA. However, the TD-AMS-PMF analysis resolved factors not resolved in the AMS-PMF analysis which is likely due to the combined impact of increasing the variance in the composition of OA and introducing a volatility dimension into the PMF analysis. The expanded content of information provided in the TD-AMS-PMF analysis also appears to allow PMF to more completely discriminate among the various OOA components identified during SOAR-1. Due to both the resolution of additional and more refined factors relative to the AMS-PMF solution, we select our final solution from the TD-AMS-analysis.

Choice of best TD-AMS-PMF solution

The correct number of factors (*p*) in a real dataset is unknown and selecting the best modeled number of factors is the most critical, and controversial, challenge in interpreting PMF results . A number of mathematical criteria have been proposed to aid the user in selecting the best solution. The most commonly used criteria in PMF analyses is the value of *Q*. If the number of factors closely approximates the number of underlying factors in the data, then *Q* should be approximately equal to the number of

points in the data matrix (Q_{exp}) and such results are a good starting point for more detailed determination of solution validity . The ratio of Q/Q_{exp}, therefore, should approach unity as the number of factors approximates the number of underlying factors . In the case of Q/Q_{exp} from the TD-AMS-PMF analysis (Fig. S1a), the value of Q/Q_{exp} decreases only slightly as the number of factors is increased throughout the investigated range of solutions and has a minimum value (2.09) in the 12-factor solution. Because Q/Q_{exp} does not display a clear minimum and universally decreases with each increase in factor numbers, this metric offers little assistance to the user in determining the correct number of factors in this case. This was similarly noted in the analysis of as well.

While other mathematical criteria have been proposed, determining the correct number of factors is ultimately at the discretion of the user depending on the number of factors that can be physically justified. To identify potential candidate solutions, the analysis of synthetically constructed OA data suggest as a preliminary guide a balance between the resolution of unique factors and factor splitting as *p* is increased . The physical justification of factors resolved in these candidate solutions must then be considered in detail using measurements external to the PMF analysis (e.g., correlating factor TS with those of known tracer species, etc.) which is also critical in assigning OA components/sources to the factors resolved by PMF . We apply this framework to the TD-AMS-PMF solutions shown in Fig. S2a.

Unique factors and corresponding OA components are resolved as the number of factors is increased from two to seven. Solutions with less than seven factors

therefore are not likely to best describe the composition of OA are not considered further. In terms of OA composition, the 7- and 8-factor solutions are essentially identical even though the number of factors increases because the additional factor in the 8-factor solution contributes to cLV-OOA. Because the 7- and 8-factor solutions are essentially identical in terms of OA composition, we discount the 7-factor solution from further consideration. A unique factor is resolved in the 9-factor solution which is also present in the 10- and 11-factor solutions. Incrementally increasing the number of factors beyond nine resolves factors that are not unique but instead are contributors to to the cLV-OOA component. Indeed, the 9- through 11-factor solutions are essentially identical despite the different number of factors in each case. Due to the lack of difference in OA composition between the 10- and 11-factor solutions, we do not consider the 11-factor solution further. Using this process of elimination, our candidates for the solution which best describes the composition of OA are those containing eight, nine, or ten factors.

In order to fully understand the difference between each of these solutions, we compare TS and MS of corresponding factors resolved therein. Component TS obtained from the 8- and 9-factor solutions are compared in Fig. S4. Individual component TS obtained from the 8-factor solution are shown in the panels to the left along with those of highly correlated external tracer species for comparison. TS of components identified from the 8- and 9-factor solutions are directly compared in the scatter plots on the right. Note that the TS of the two MV-OOA subcomponents resolved in the 9-factor solution were combined to allow comparison with the 8-factor

solution. There is little difference between TS of HOA and LOA components as each have an $r^{TS} \geq 0.99$. In contrast, correlation of OOA component TS are substantially lower ranging from 0.82 to 0.97. Interestingly, the highest correlation among the OOA TS is obtained from comparison of MV-OOA despite recombination in the case of the 9-factor solution subcomponents.

Similarly, MS of these components resolved in the 8- and 9-factor solutions are compared in Fig. S5 which is analogous to Fig. S4. Full MS shown on the left were those of the 8-factor solution which are compared with those from the 9-factor solution on the right. EA results and f_{44} of the 8-factor component MS are also reported. MS of the two MV-OOA subcomponents resolved in the 9-factor solution have been recombined. As the scatterplots show, MS obtained from the different solutions are very similar for the most part, particularly in the case of HOA and the LOA components. Among the OOA components, cLV-OOA and MV-OOA appear to have a higher degree of similarity than SV-OOA. Despite their similarity, the intensity of CO_2^+ is substantially different between the 8- and 9-factor solution spectra, particularly in the case of LOA-AC, MV-OOA, and SV-OOA.

Fig. S6 and S7 compares TS and MS, respectively, obtained from the 9- and 10-factor solutions. TS and MS of components resolved from the 10-factor solution are shown in the panels on the left side of each figure along with the corresponding results of EA and f_{44} while MS and TS of the 10-factor components are compared against those of the 9-factor solution on the right. The correlation between TS obtained from the 9- and 10-factor solutions, including those of the OOA factors, is much higher than

between the 8- and 9-factor solutions with all TS having $r^{TS} \geq 0.99$. Similarly, Fig. S7 shows the same is true of factor MS as well including the intensity of CO_2^+ in each spectrum.

CO_2^+ has a large influence on f_{44} and the O/C ratio obtained from EA, both of which can be used to characterize the oxidation of OA including those components resolved through PMF analysis. Due to its large magnitude in AMS OA spectra, particularly those of OOA components, O/C and f_{44} are highly sensitive to the magnitude of CO_2^+. The impact of CO_2^+ on both can be seen in Fig. S7 where O/C and f_{44} for the mass spectra obtained from the 8- and 10-factor solutions are plotted against those obtained from the 9-factor solution. Both the O/C ratio and f_{44} for factors isolated from the 8-factor solution are substantially different from those of the 9-factor solution largely due to the large variation in the intensity of the CO_2^+ fragment between each set of spectra. This is particularly true for LOA-AC and MV-OOA, which exhibited the largest difference in the magnitude of the CO_2^+ ions. Although the magnitude of CO_2^+ is also different in the SV-OOA factor spectrum, it is likely that the impact of CO_2^+ on O/C and f_{44} is mitigated in this case due to the contribution of additional oxygenated ions to its MS. As expected based on the similarity of CO_2^+ ion intensities in MS obtained from the 9- and 10-factor solutions, f_{44} and O/C ratios of factors identified in these solutions are nearly identical. The detailed examination of the TS and MS of factors resolved from the 8-, 9-, and 10 solutions reveals a large degree of change in both as the number of factors included in the solution increase from eight to nine while there is virtually no

change as the number increase from nine to ten. As a result, we dismiss the 10-factor solution from further consideration as it is virtually identical to the 9-factor solution.

As a result, the only candidate for the solution that best represents SOAR-1 OA composition is either the 8- and 9-factor solution which differ only in the resolution of two different subcomponents of MV-OOA as the number of factors is increased to nine,. Ultimately, the choice among the 8- and 9-factor solutions ultimately rests with whether the additional factor resolved in the latter solution can be physically justified and not merely an artifact of the factorization (e.g., from factor splitting). If the factor representing the subcomponents of MV-OOA resolved in the 9-factor solution were due to factor splitting, they would have similar TS and MS . As Fig. S6d and S6e show, TS of these factors are quite similar. However, MS of these factors (ref. Fig. S7e and S7f) are substantially different as is the results of EA and f_{44} for each spectrum. The fact that these components have substantially different MS argues against their arising from from factor splitting. This conclusion is additionally supported by difference in the relative volatility of the two components. Volatility profiles for factors resolved in the 9-factor solution are shown in Fig. S20. Overall, these profiles are similar to those reported by which were obtained for factors resolved in the 8-factor solution. Profiles of the two MV-OOA subcomponents are provided in Fig. S20e and show that these factors indeed have different relative volatilities. Finally, we note that that the newly-resolved subcomponents of MV-OOA appear to obtain mass from multiple components in the 8-factor solution, which is again uncharacteristic of factor splitting. As a result of these considerations, we are disinclined to think that the subcomponents of MV-OOA arise

from factor splitting and have chosen the 9-factor (7-component) solution as the best model of OA composition during SOAR-1. This solution and the assignment of each factor therein to a unique OA component are discussed in detail in the main text.

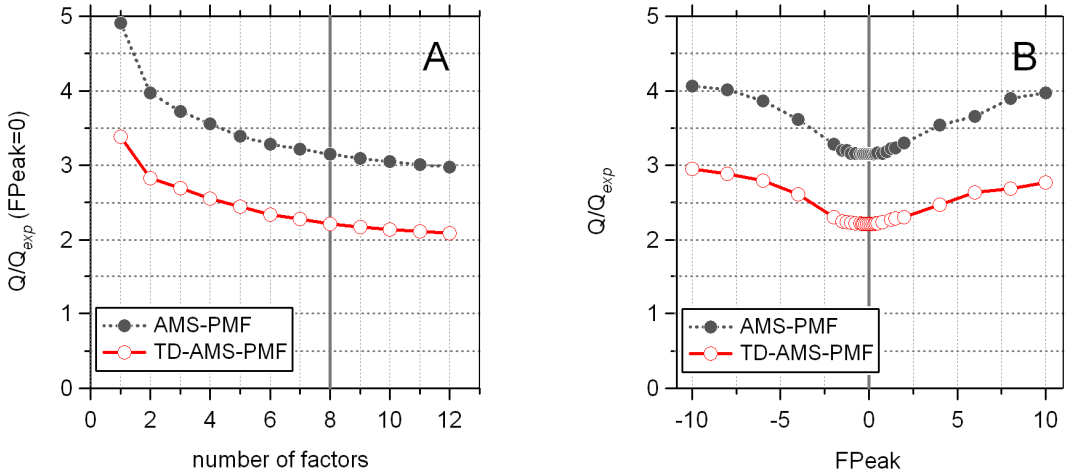

Figure S1. Q/Q_{exp} obtained from both AMS-PMF and TD-AMS-PMF analyses. Fig. S1a shows Q/Q_{exp} as a function of the number of factors in the solution while Fig. S1b shows Q/Q_{exp} from the 8-factor (6-component) AMS-PMF and TD-AMS-PMF solutions as a function of Fpeak.

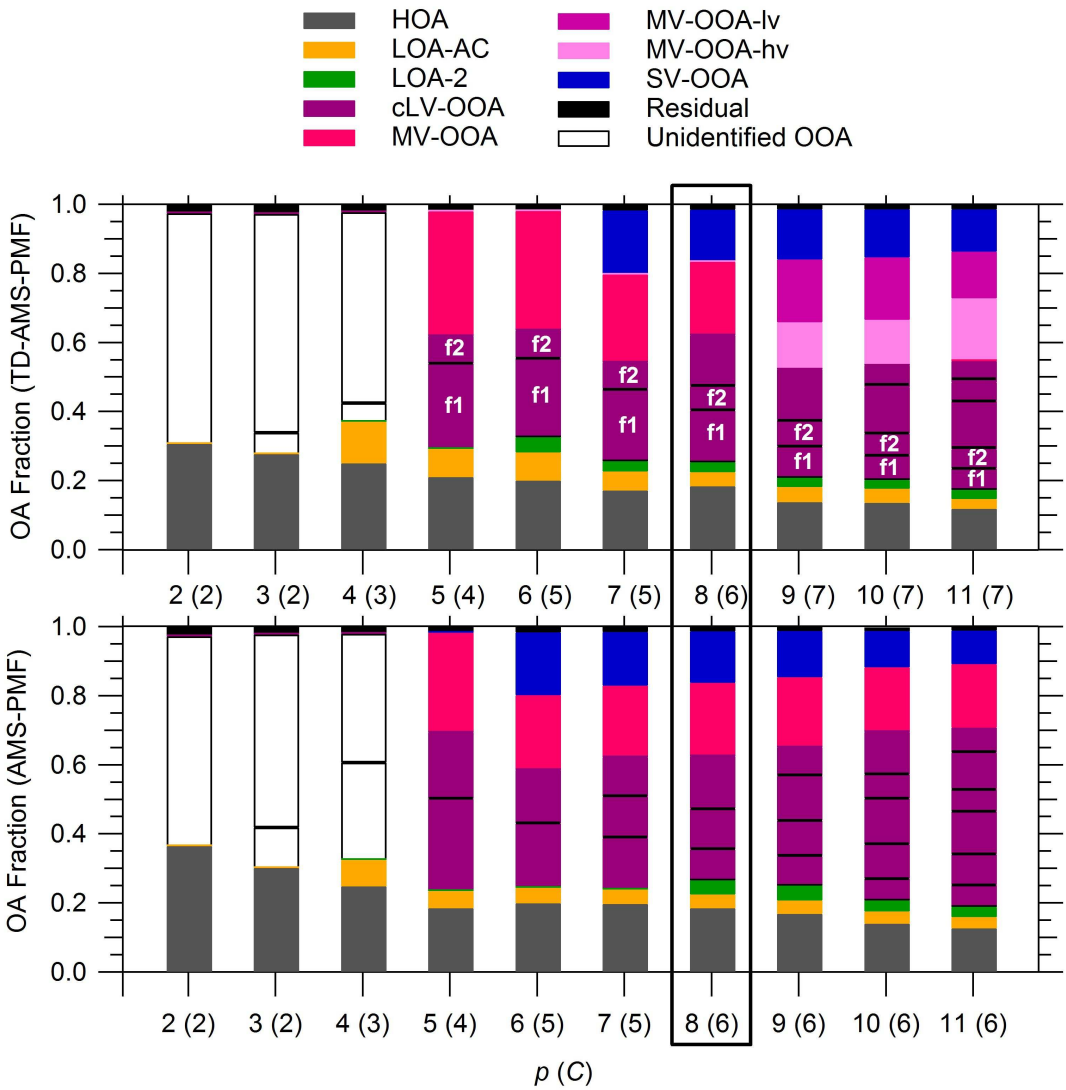

Figure S2. Results from TD-AMS-PMF and AMS-PMF analyses. Each plot shows the relative contributions of both PMF factors and corresponding identified OA component as a function of the number of factors (*p*) and the number of components (*C*). As described in the text, *p* and *C* differ in the majority of investigated solutions due to factor recombination in the case of cLV-OOA (represented by the horizontal black lines). Overall, 6-component solutions from both analyses resolve similar factors and components. The 6-component solutions are compared in greater detail in order to explore the benefit of including thermally-denuded HR-AMS data in PMF analysis.

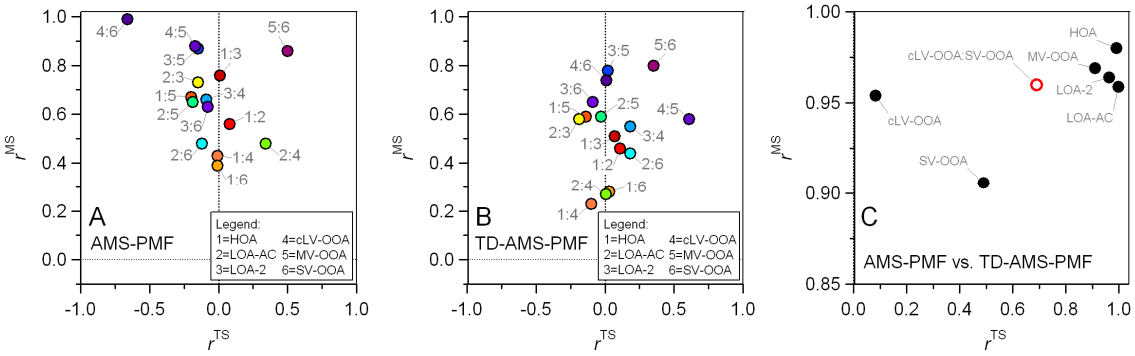

Figure S3. Plots summarizing r^{TS} and r^{MS} among components identified within both the 8-factor (6-component) AMS-PMF (Fig. S3a) and TD-AMS-PMF (Fig. S3b) solutions and also between each solution (Fig. S3c). Generally, r^{TS} and r^{MS} among components of the TD-AMS-PMF solution are lower that those of the AMS-PMF components indicating a greater degree of dissimilarity and improved resolution of the various components. When comparing results between each solution, TS and MS of the majority of OA components are very similar with the exception of cLV-OOA and SV-OOA. This difference is largely eliminated, however, when the cLV-OOA and SV-OOA components (cLV-OOA:SV-OOA) is combined.

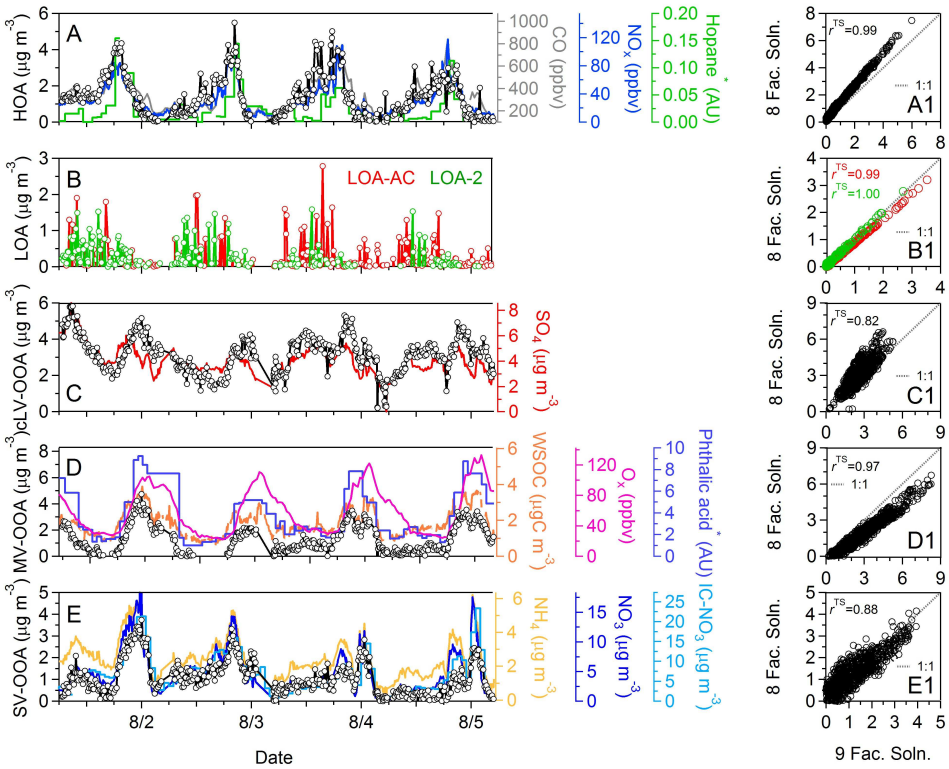

Figure S4. Comparison of 8- and 9-factor TD-AMS-PMF OA component time series. Time series obtained from the 8-factor solution are shown in Figs. S4a-S4e along with those of highly correlated tracer species. 8- and 9-factor component time series are compared in Figs. S4a1-S4e1. In order to directly compare MV-OOA factors between the two analyses, the MV-OOA subcomponents identified in the 9-factor solution were combined. In general, time series of HOA and LOA components are much more highly correlated than those of the resolved OOA components.

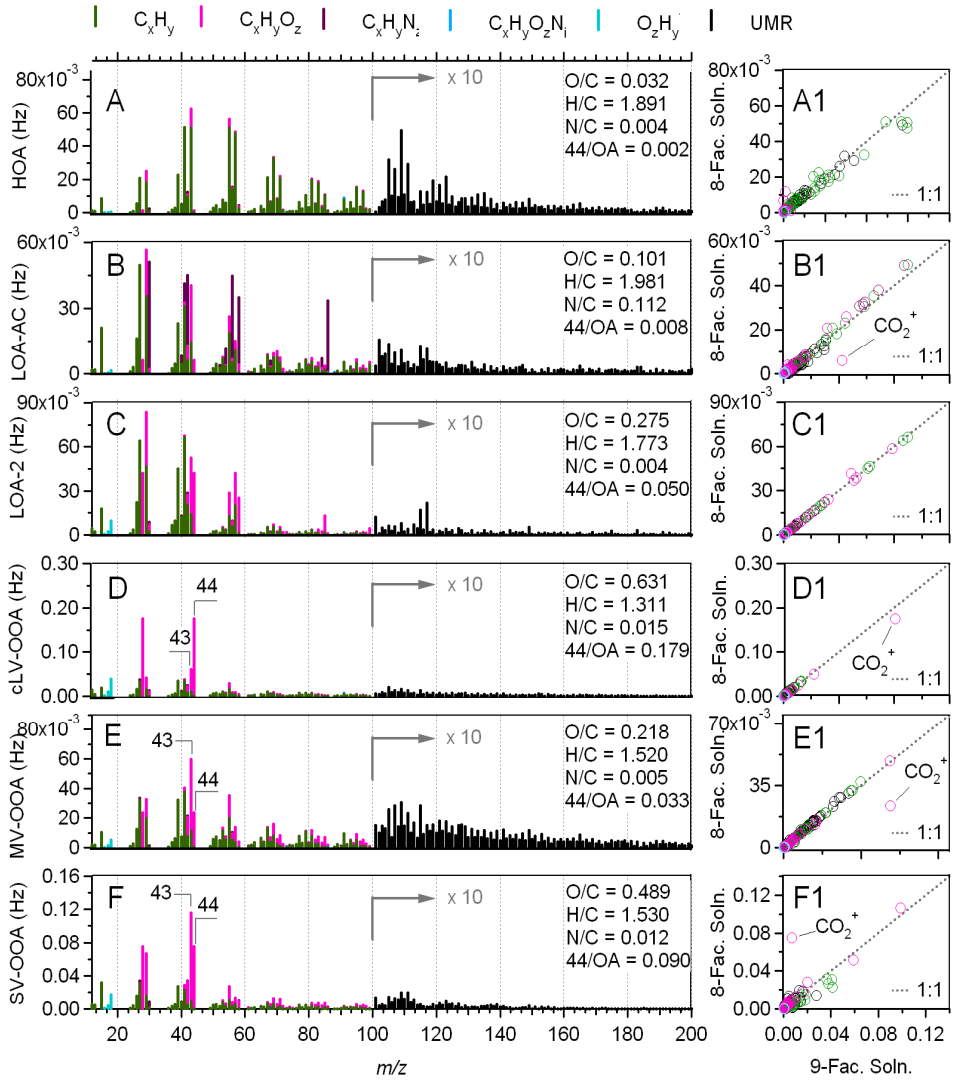

Figure S5. Comparison of 8- and 9-factor TD-AMS-PMF OA component mass spectra. Mass spectra obtained from the 8-factor solution are shown in Figs. S5a-S5f and are plotted against those obtained from the 9-factor solution in Figs. S5a1-S5f1. In order to directly compare MV-OOA, the two MV-OOA factors identified in the 9-factor solution were combined. In general, mass spectra of HOA and LOA-2 obtained from the different solutions display only minor differences relative to those of LOA-AC and the identified OOA components, which exhibit substantial differences, particularly in the contribution of CO_2^+.

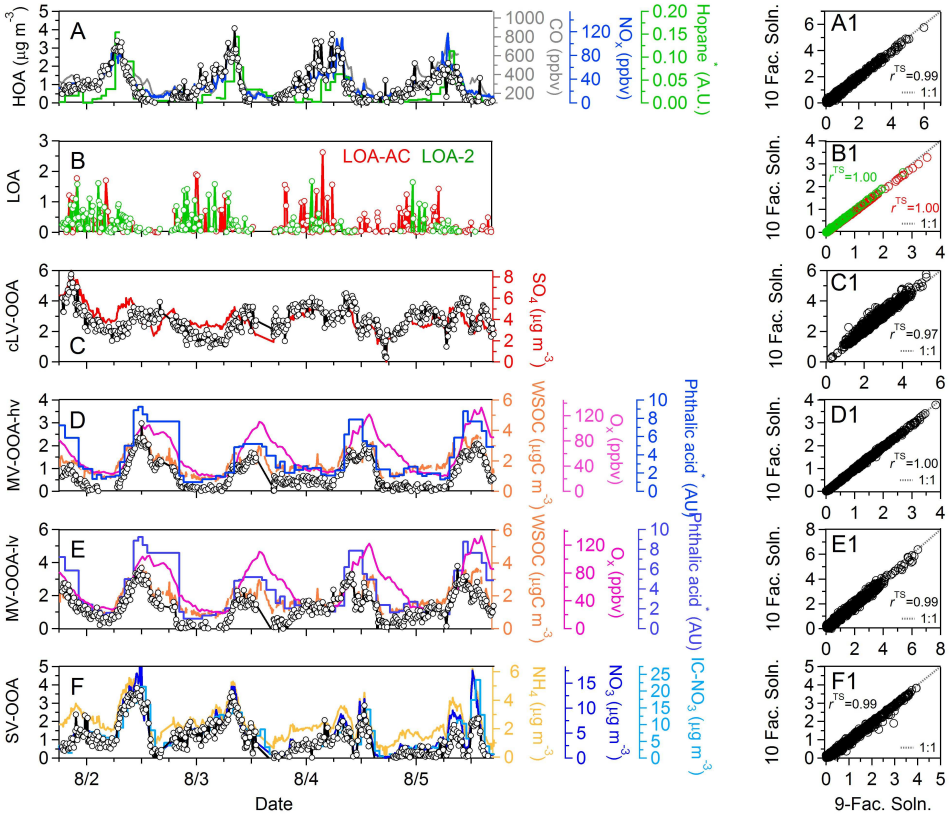

Figure S6. Comparison of 9- and 10- factor TD-AMS-PMF OA component time series. Time series obtained from the 10-factor solution are shown in Figs. S6a-S6f along with those of highly correlated tracer species. OA component time series from the 10-factor solution are plotted versus those of the 9-factor solution in Figs. S6a1-S6f1. Component time series, in this case, are highly correlated indicating little change as the number of factors is increased beyond nine thereby suggesting the stability of the PMF solution.

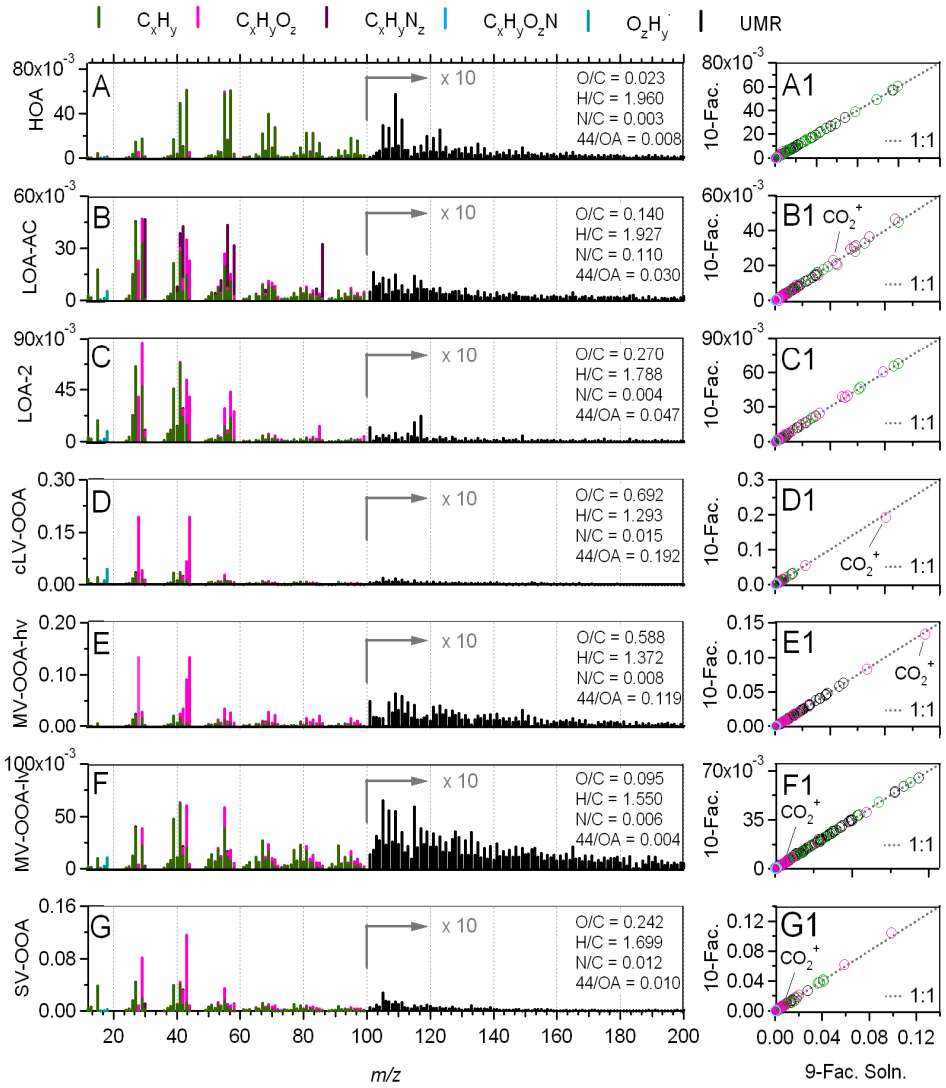

Figure S7. Comparison of 9- and 10-factor TD-AMS-PMF OA component mass spectra. Mass spectra of components obtained from the 10-factor solution are shown in Figs. S7a-S7f and are directly compared with those from the 9-factor solution in the Figs. S7a1-S7f1 scatter plots. Similar to the comparison of component time series obtained from these solutions, MS of these components are highly correlated, indicate little change, and suggest stability of the PMF solution.

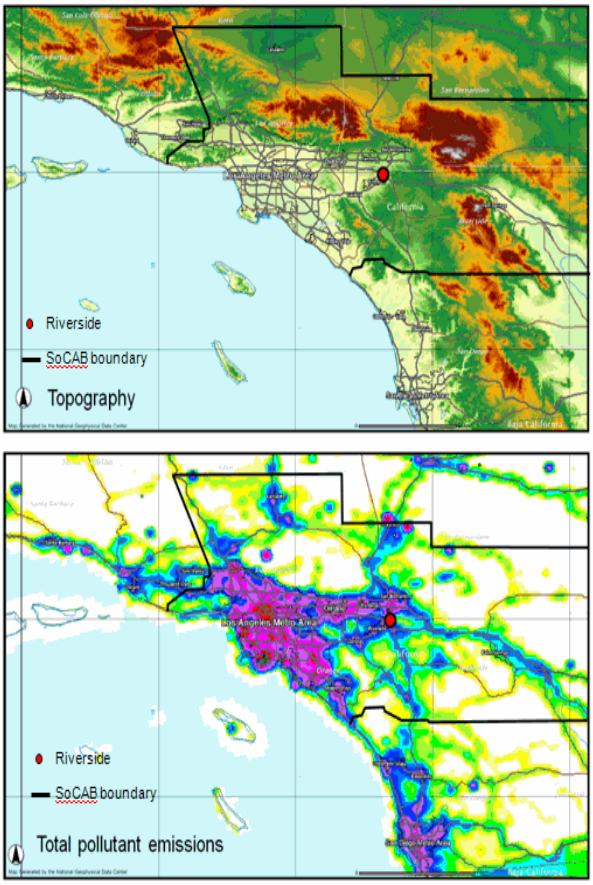

NOAA National Emission Inventory (http://map.ngdc.noaa.gov/website/al/emissions/viewer.htm)

Figure S8. Topography and total pollutant emission maps of the SoCAB region of Southern California. The SOAR-1 sampling site at UC-Riverside is noted by the red dot on each map.

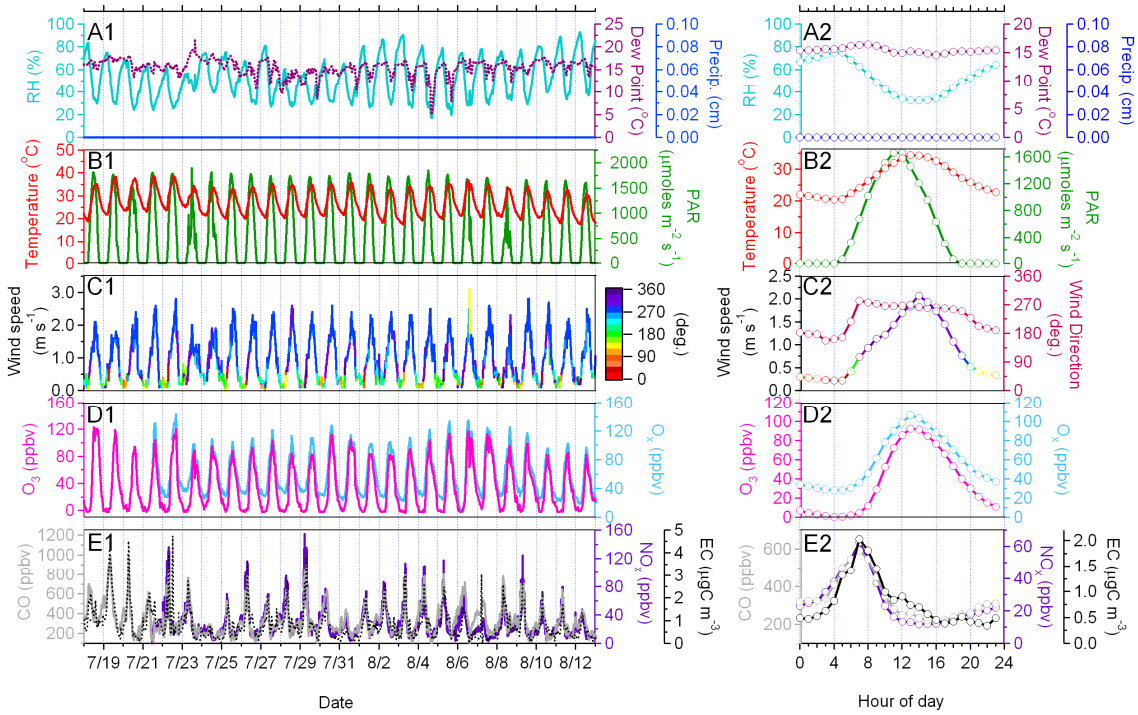

Figure S9. TS (left) and diurnal profiles (right) of meteorological conditions (RH, temperature, wind speed and direction), gas-phase species (O_3, O_x, CO, and NO_x), and EC during SOAR-1. Note that CO concentrations in Figs. E1 and E2 have been offset vertically to account for a CO background of 100 ppb.

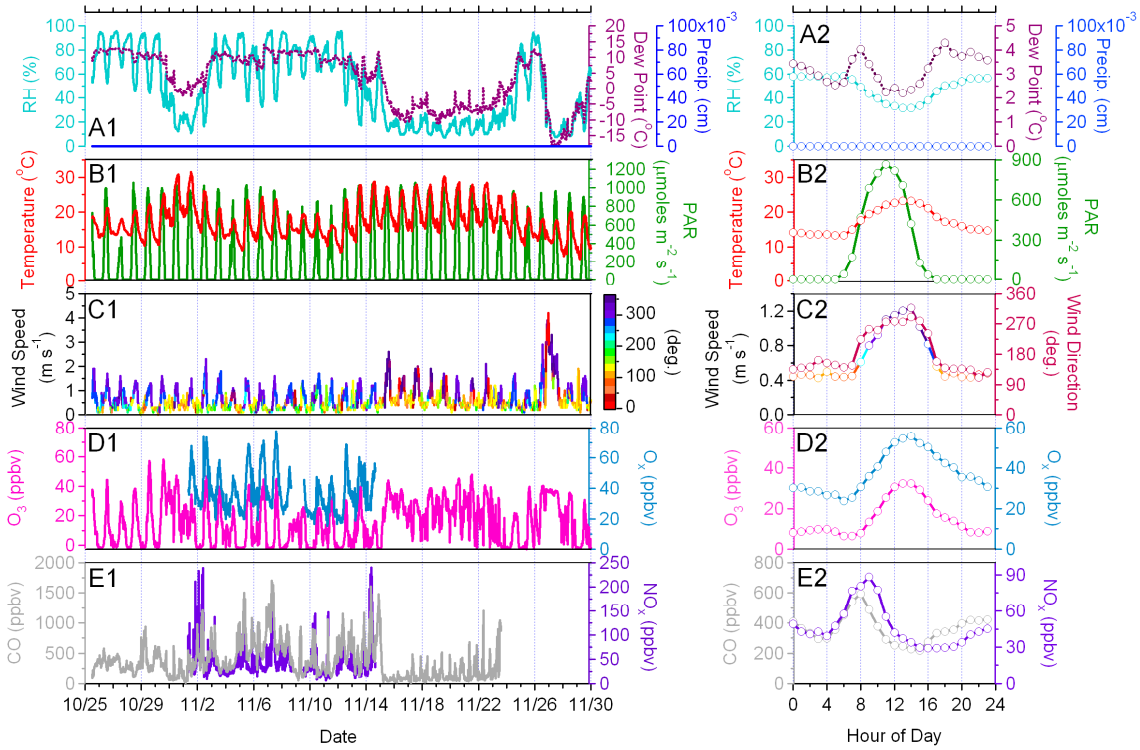

Figure S10. TS (left) and diurnal averages (right) of meteorological conditions (RH, temperature, wind speed and direction), gas-phase species (O_3, O_x, CO, and NO_x), and EC during SOAR-2. Note that CO concentrations in Figs E1 and E2 have been offset vertically to account for a CO background of approx. 100 ppb.

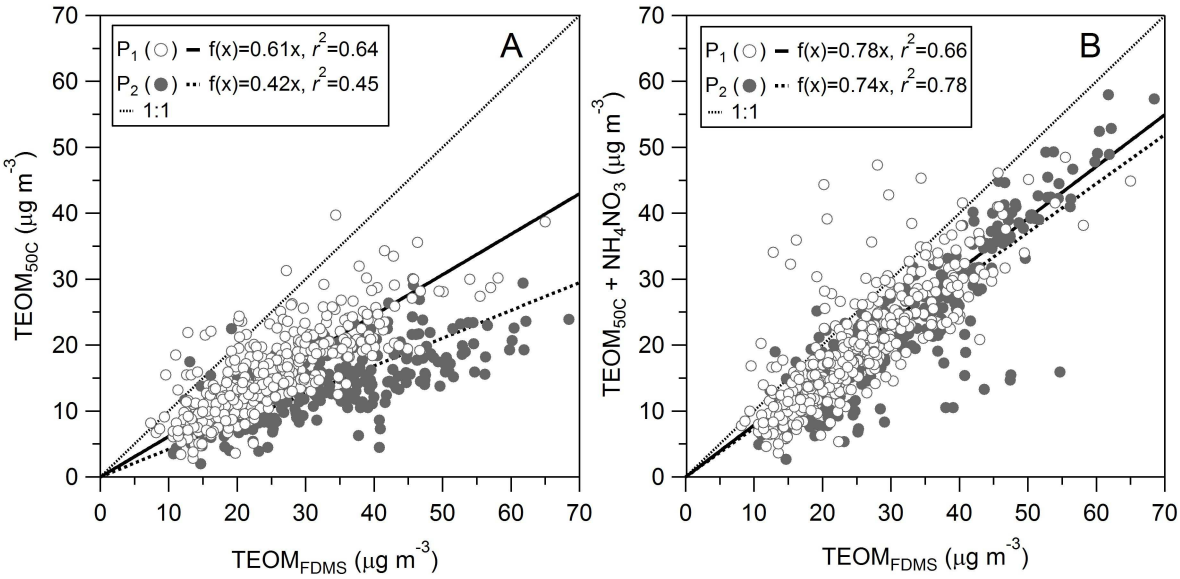

Figure S11. Comparison of TEOM measurements as reported, and after adding estimated NH_4NO_3 concentrations. $TEOM_{50C}$ measurements are plotted against $TEOM_{FDMS}$ in Fig. S11a while $TEOM_{50C}$ supplemented by calculated NH_4NO_3 mass are plotted against $TEOM_{FDMS}$ measurements in Fig. S11b along with the results of linear regression and correlation coefficients in both cases. Open symbols represent period P1 (7/18-8/1/2005) while filled symbols represent P2 (8/2-8/13/2005) measurements.

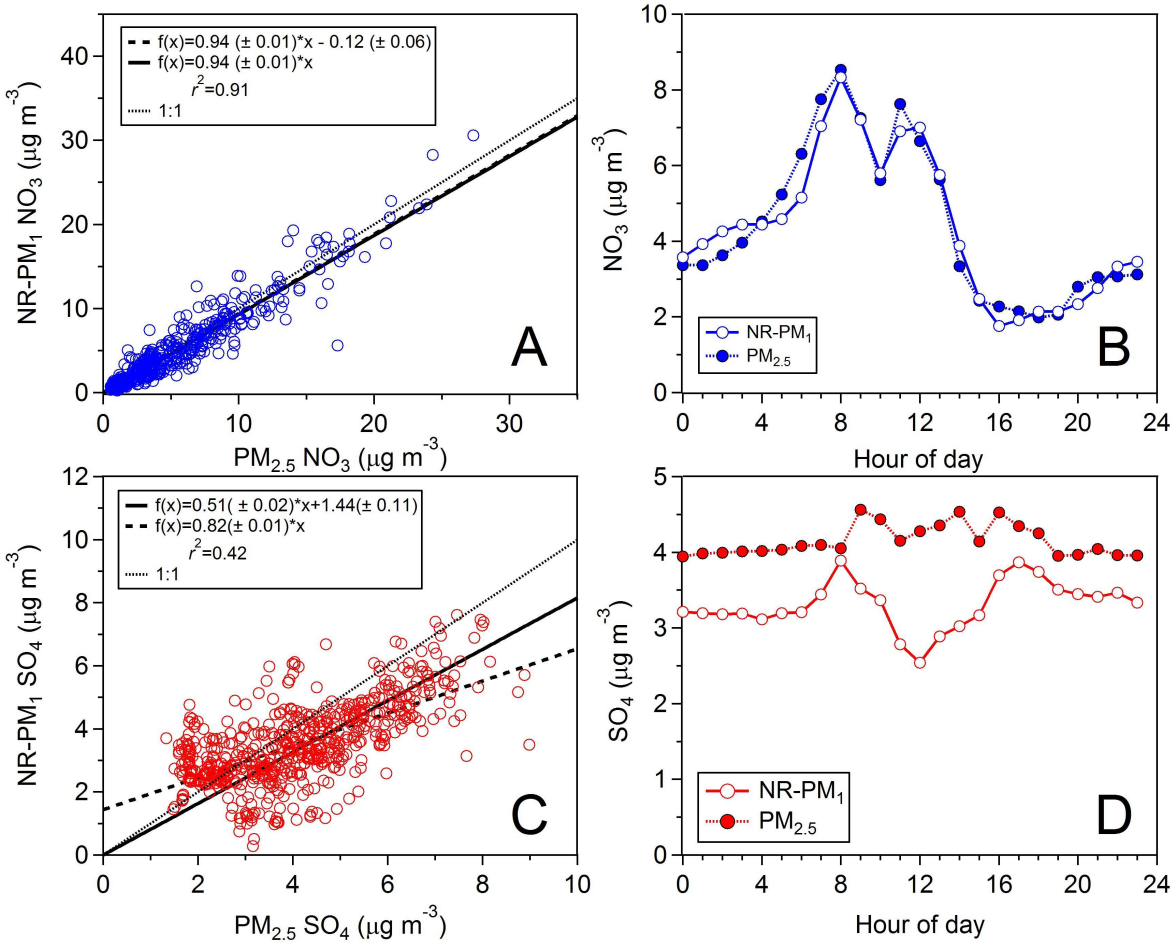

Figure S12. Comparison of NR-PM_1 and $PM_{2.5}$ NO_3 and SO_4 concentrations throughout the duration of SOAR-1. NR-PM_1 NO_3 and SO_4 concentrations obtained from the HR-AMS are plotted against corresponding IC-nitrate and IC-sulfate measurements in Figs. S12a and S12c, respectively, along with results of linear regression and correlation coefficients (r^2). Average diurnal profiles for both NR-PM_1 and $PM_{2.5}$ NO_3 and SO_4 measurements are also shown in Figs. S12b and S12d, respectively.

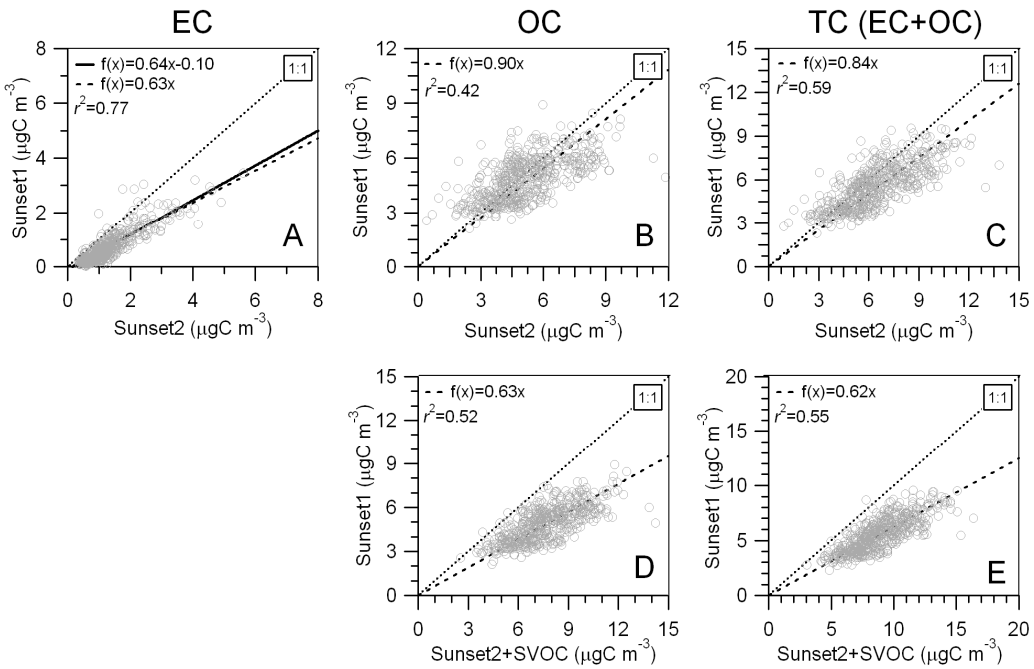

Figure S13. Comparison of EC, OC, and total carbon (TC, i.e., EC+OC) measured by Sunset1 and Sunset2 and Sunset2+SVOC.

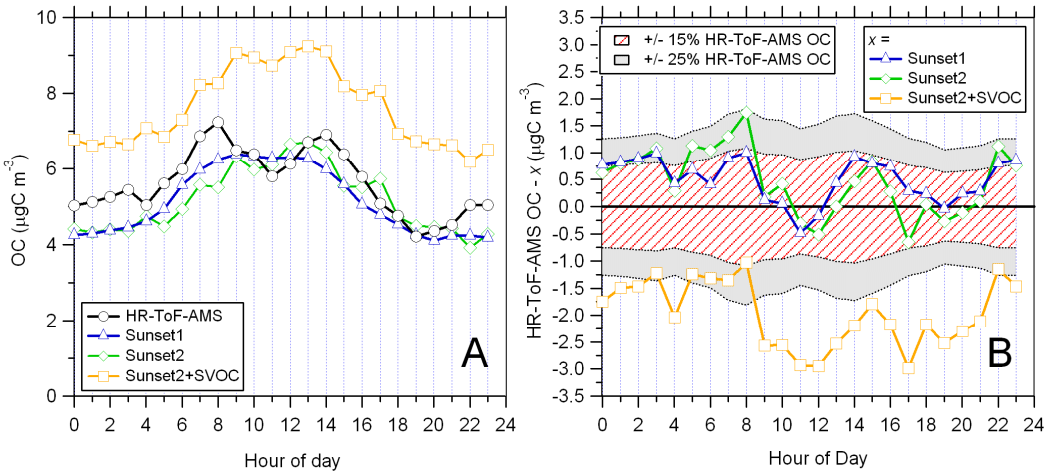

Figure S14. Diurnal profiles of HR-AMS and Sunset OC measurements. Diurnal averages are shown in Fig. S14a while profiles of difference between HR-AMS and Sunset measurements (i.e., HR-AMS OC – Sunset OC) are shown in Fig. S14b, along with bands that represent +/-15% and +/-25% of the HR-AMS OC.

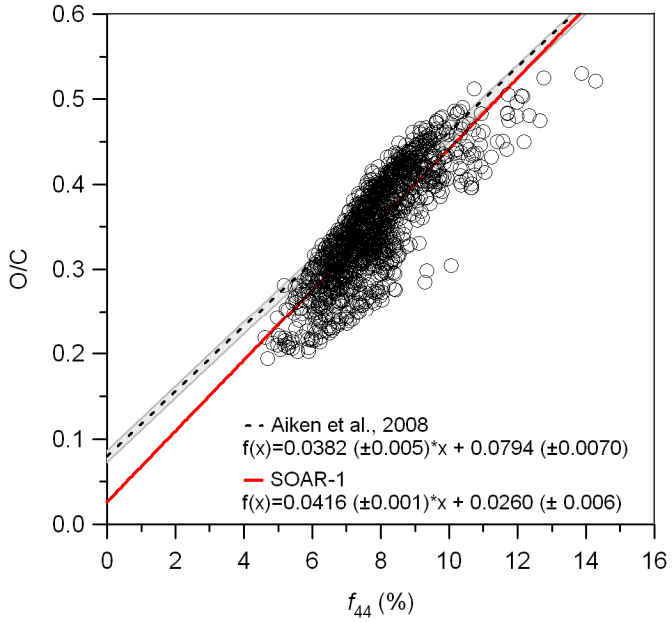

Figure S15. Scatter plot of f_{44} vs. O/C derived from HR-AMS high-resolution data during SOAR-1. Results in linear regression of SOAR-1 data are shown along with similar results from Aiken et al. (2008) for comparison.

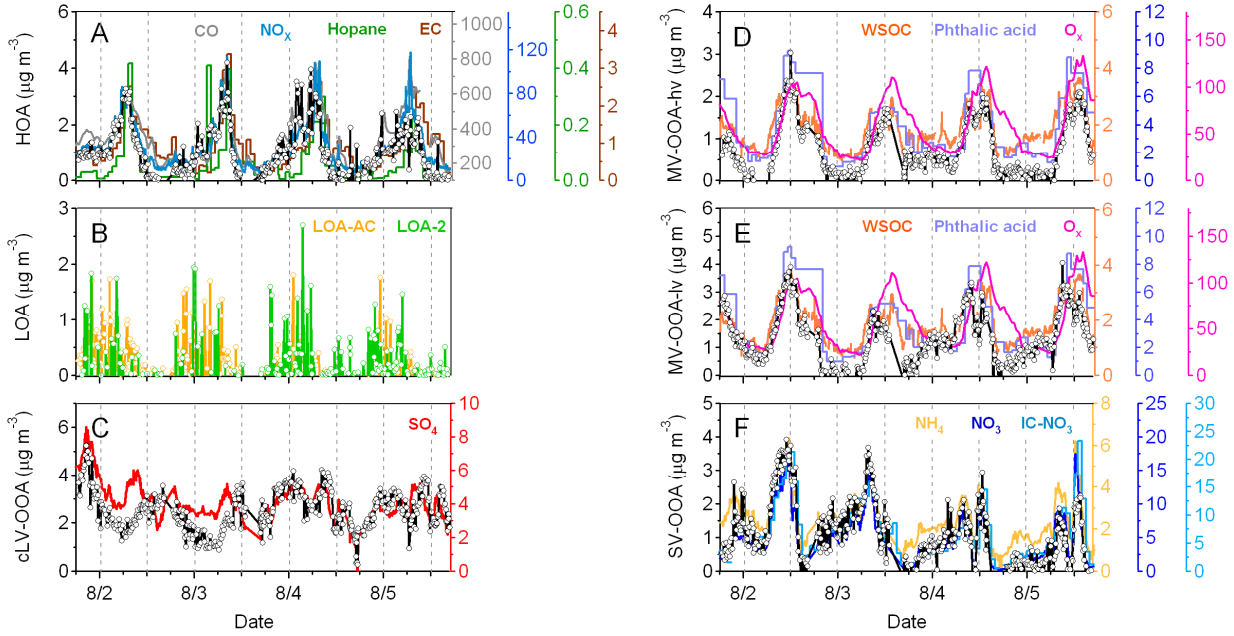

Figure S16. TS of OA components identified from the 7-component TD-AMS-PMF solution. TS of highly correlated primary, secondary, or inorganic tracer species have also been included for visual reference.

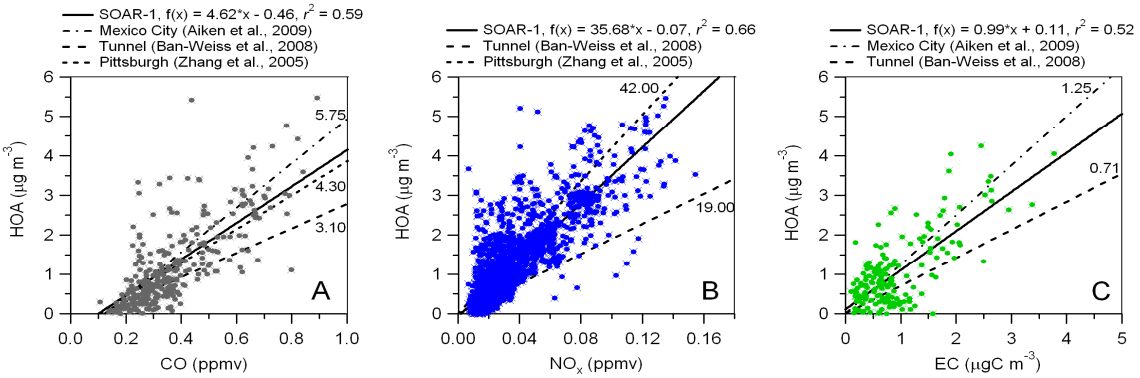

Figure S17. Scatter plots of HOA time series with those of select primary marker species CO (Fig. S17a), NO_x (Fig. S17b), and EC (Fig. S17c). Results of linear regression are also shown along with those of previous studies in a variety of locations including Mexico City, Pittsburgh, and the Caldecott Tunnel.

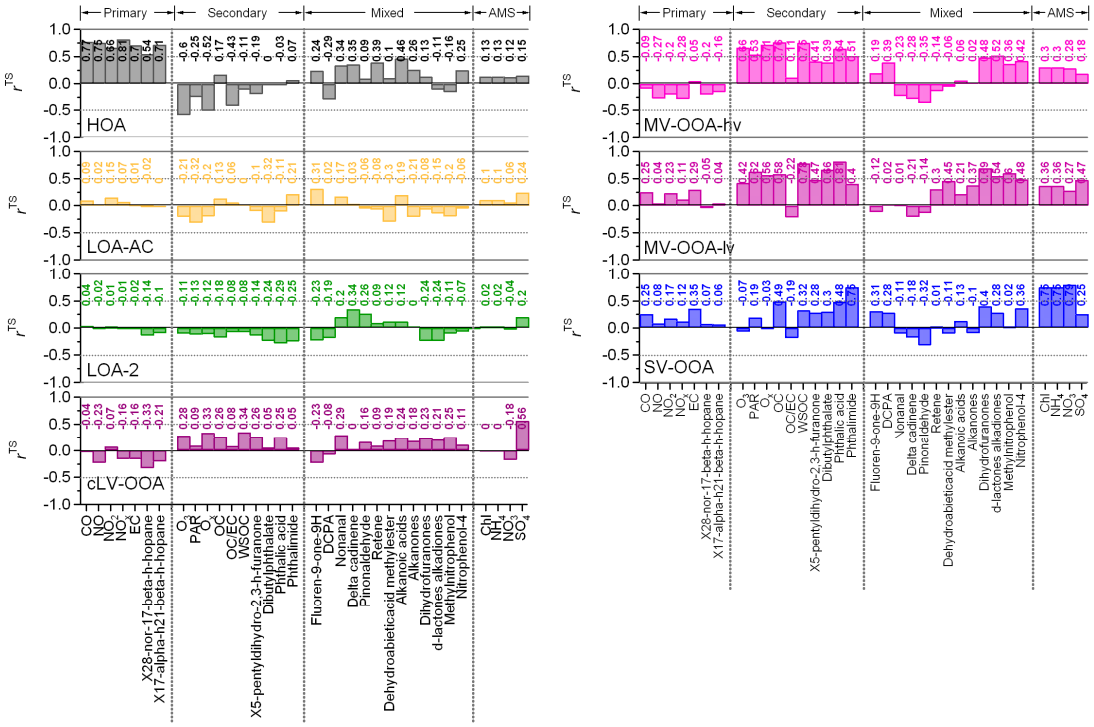

Figure S18. Correlations (r^{TS}) from comparison of 7-component TD-AMS-PMF component TS with those of tracers measured during SOAR-1. Tracers have been grouped according to type (e.g., primary, secondary, mixed, and inorganic) on the horizontal axis in order to highlight trends.

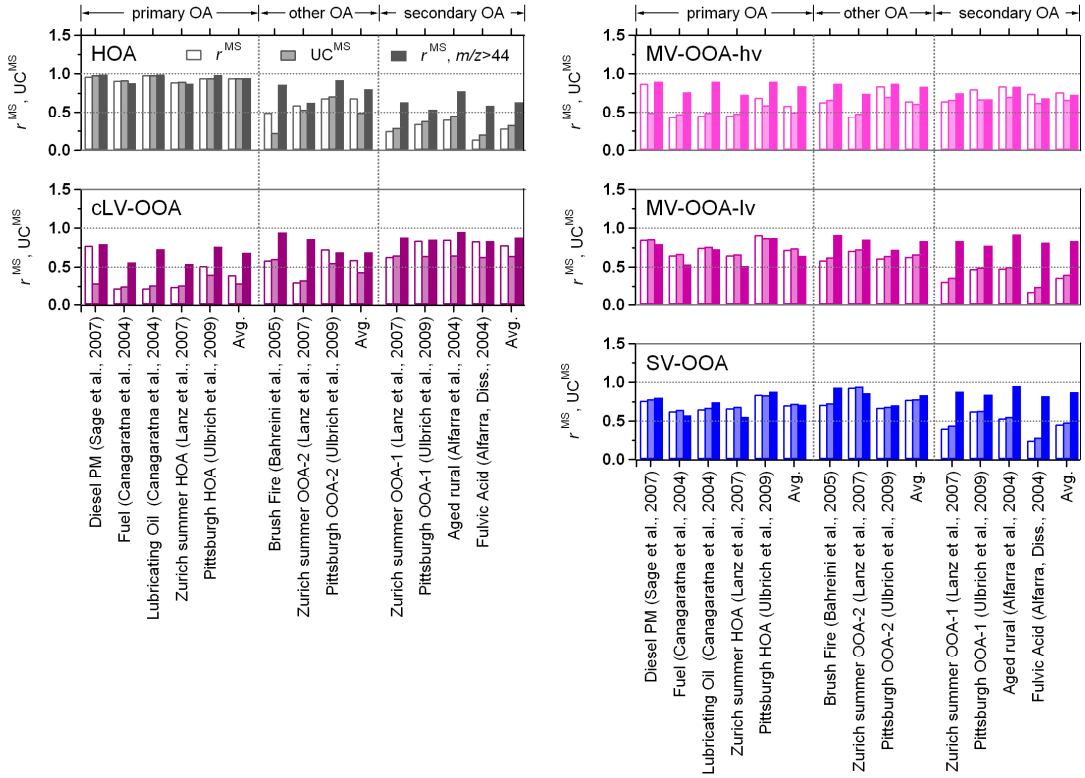

Figure S19. Correlations (r^{MS}, UC^{MS}) between 7-component TS-AMS-PMF component MS and standard MS. Results are not shown for the two LOA components due to the lack of comparable standards. Standard MS have been grouped according to source (e.g., primary, other, and secondary) on the horizontal axis in order to highlight trends.

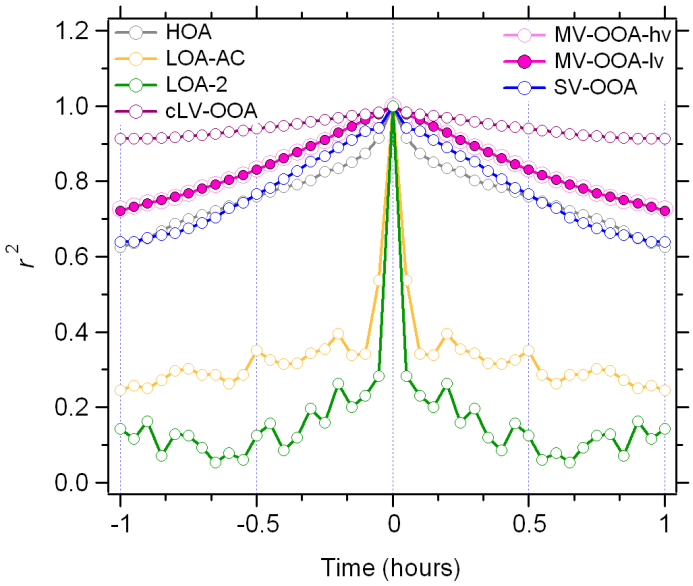

Figure S20. Auto-correlation of 7-component TD-AMS-PMF OA component TS over ±1 hour. In contrast to the relatively flat auto-correlation profiles for the majority of components, those of the LOA components display sharp profiles in the center of this range indicating the highly variable nature of time series for these components.

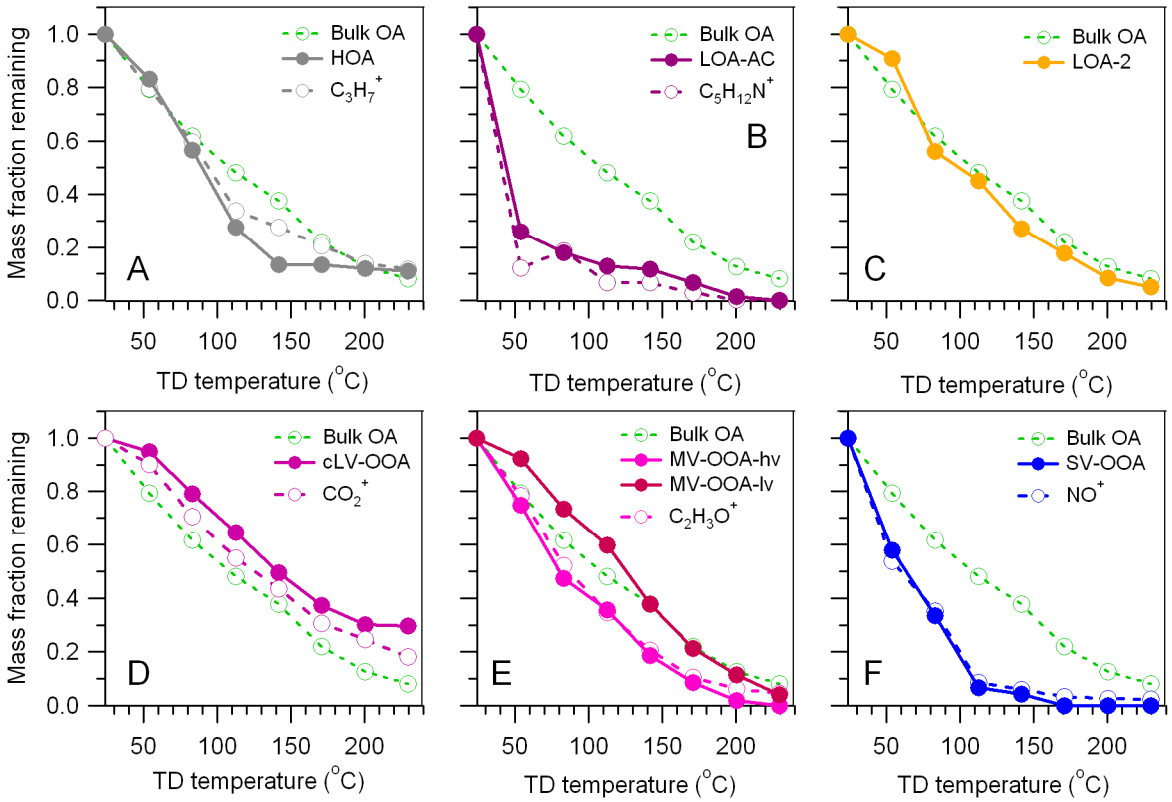

Figure S21. Relative volatilities of components resolved in the 7-component TD-AMS-PMF solution. Relative volatilities of individual ions that are either considered markers of individual OA components (e.g., $C_3H_7^+$ in Fig. S21a), are prominent in the component MS (e.g., $C_5H_{12}N^+$ in Fig. S21b), or which exhibit similar volatility characteristics (e.g., NO^+ in Fig. S21f) are shown along with a that of bulk OA for reference.

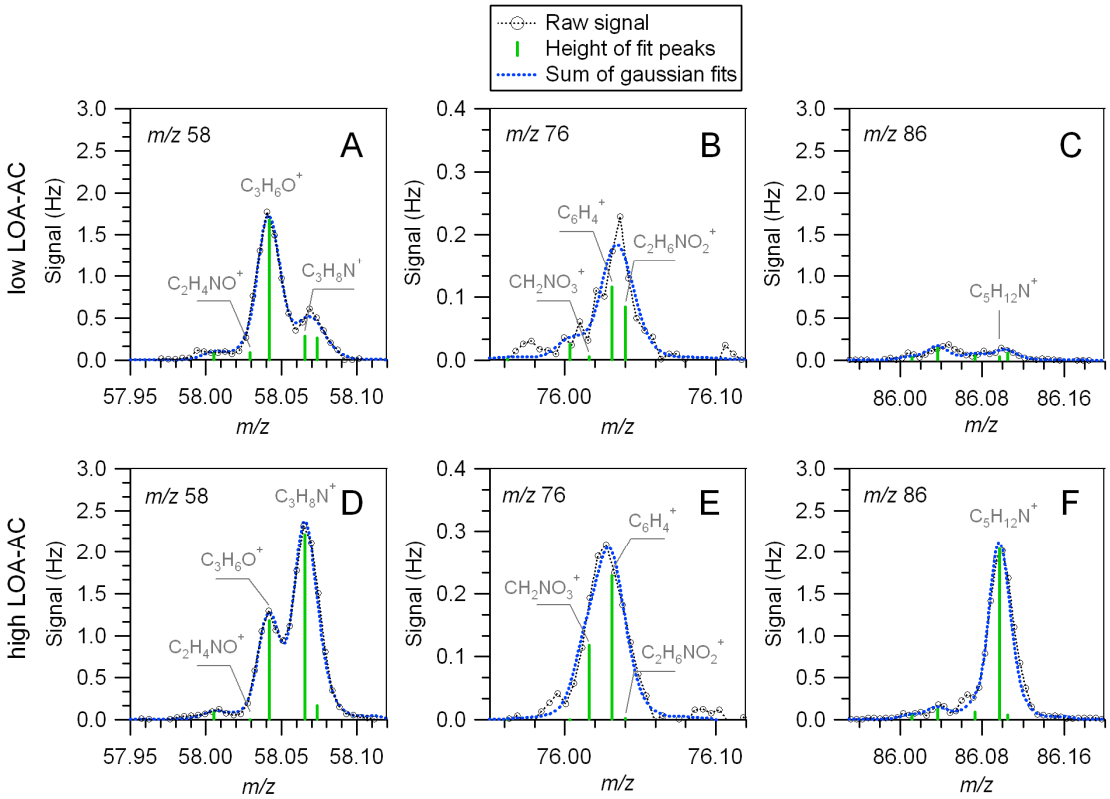

Figure S22. Raw mass spectra of characteristic amine fragments (nominal *m/z* 58, 76, and 86) during periods of low and high LOA-AC concentrations. Figs. S22a-c show fragment intensities during periods of low LOA-AC concentrations while Figs. S22d-f show the same during periods of high LOA-AC concentrations. Characteristic reduced amine fragments ($C_3H_8N^+$ and $C_5H_{12}N^+$) are higher during periods of high LOA-AC concentrations with small associated increases in the concentration of oxidized amine fragments ($C_2H_4NO^+$ and $C_2H_6NO_2^+$) identified from chamber oxidation of trimethylamine.

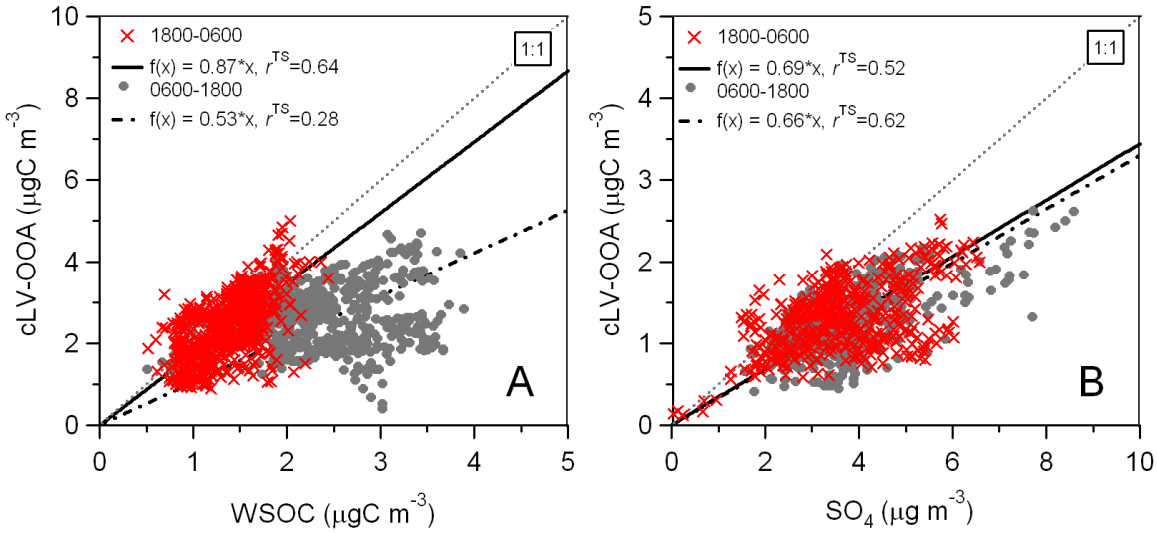

Figure S23. Relationship between daytime (0600-1800) and overnight (1800-1600) cLV-OOA time series with SO_4 and WSOC. In the case of WSOC, cLV-OOA concentrations have been converted to carbon equivalent mass concentrations using the OM/OC obtained from EA. While the relationship between cLV-OOA appear similar both during daytime and overnight periods, the relationship between cLV-OOA and WSOC within the two periods is substantially different within the two periods. cLV-OOA concentrations are more highly correlated to WSOC concentrations during overnight periods indicating contributions of additional OA components to WSOC during the day.

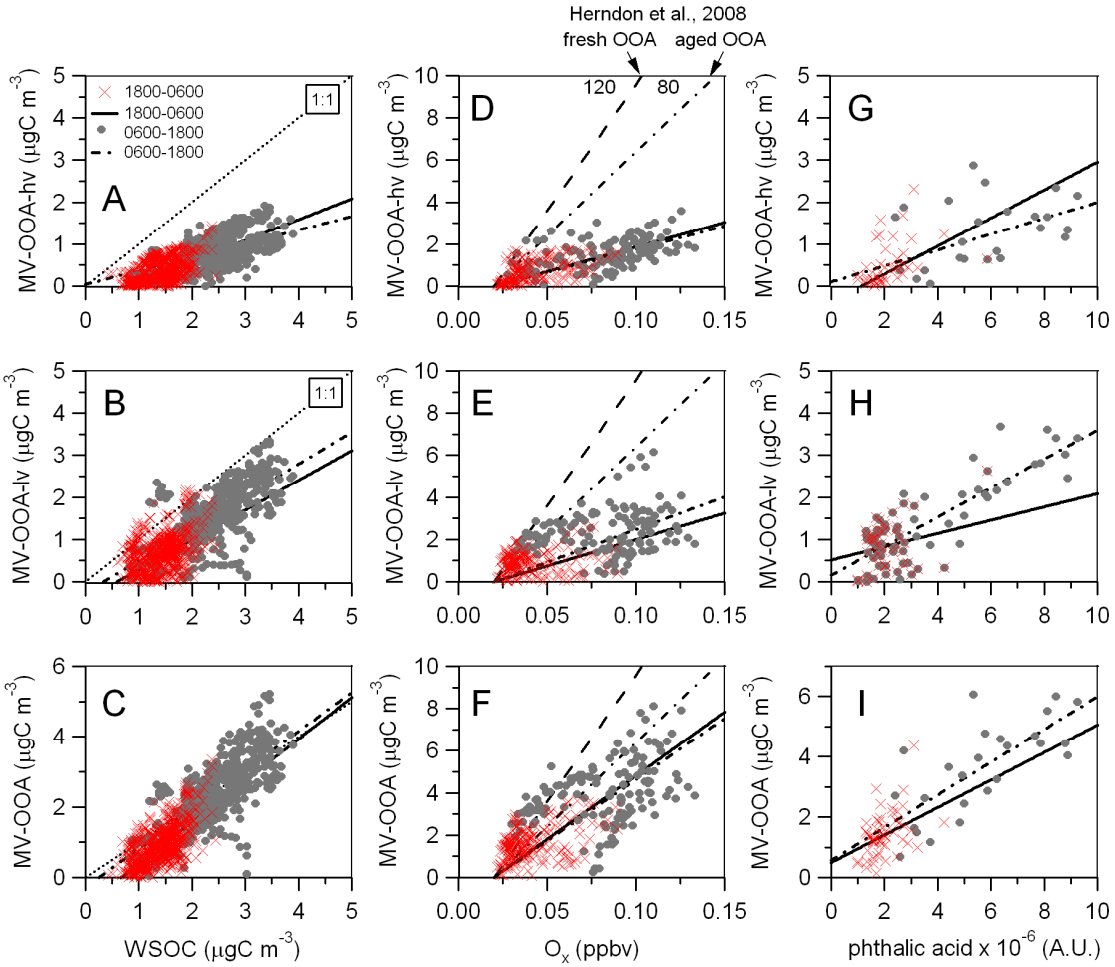

Figure S24. Relationship between MV-OOA-lv, MV-OOA-hv, and MV-OOA concentrations with secondary OA marker species WSOC (Figs. S24a-c), O_x (Figs. S24d-f) and particle-associated phthalic acid (Figs. S24g-i). Detailed results of linear regression and correlation coefficients are provided in Table 1. Results of linear regression are shown in Figs. S24d-f for reference.

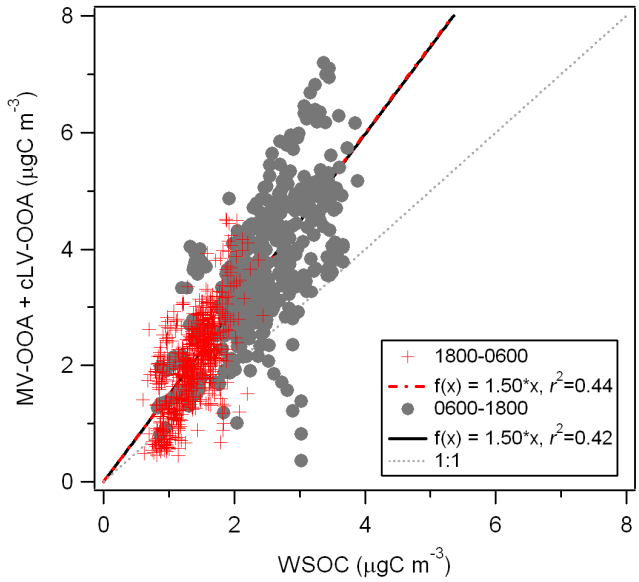

Figure S25. Sum of MV-OOA and cLV-OOA (comparable to bulk OOA) versus WSOC over the course of SOAR-1.

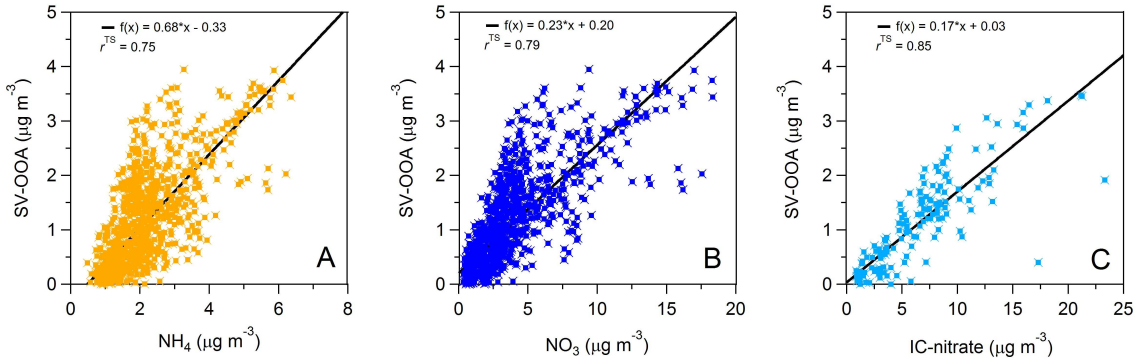

Figure S26. Relationship between SV-OOA concentrations and inorganic species including NR-PM_1 NH_4 (Fig. S26a), NR-PM_1 NO_3 (Fig. S26b), and IC-nitrate (Fig. S26c).

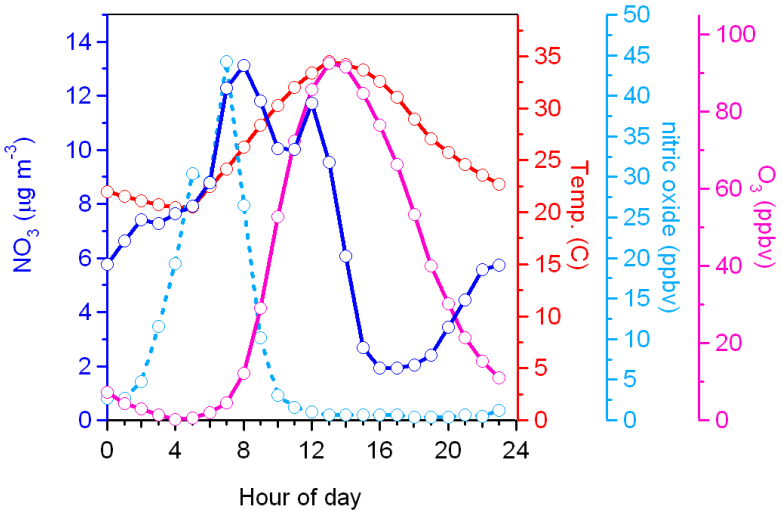

Fig. S27. Diurnal profiles of HR-AMS NO_3 along with those of gas-phase NO, O_3, and ambient temperature during SOAR-1.

Table S1. Research groups participating in SOAR along with their institution, measurements, and publications.

Group	Institution	Measurement	SOAR-1	SOAR-2	Publications including results from SOAR	Funding Sources
Arey	University of California-Riverside	$PM_{2.5}$ filter sampling	■			
Eatough	Brigham Young University	Dual-channel Sunset semi-continuous EC/OC monitor, $TEOM_{FDMS}$, $TEOM_{50C}$, PC-BOSS, IC-NO_3, IC-SO_4	■		Eatough et al. 2008; Grover et al. 2008; Eatough et al. 2009; Grover et al. 2009; Docherty et al., this paper	NSF ATM-0407695
Fitz	University of California-Riverside	$PM_{2.5}$ filter sampling	■			US EPA R831087
Goldstein	University of California-Berkeley	Thermal desorption aerosol GC/MS (TAG), GC/MS for VOC analysis CO, Ozone, meteorological measurements	■	■	Gentner et al. 2009; Kreisberg et al. 2009; Williams et al. 2010a; Gentner et al. 2010; Willaims et al 2010b; Docherty et al. 2008; Docherty et al., this paper	US EPA RD-83096401-0 CARB 03-324
Hannigan	University of Colorado-Boulder	$PM_{2.5}$ filter sampling	■			
Hering	Aerosol Dynamics, Inc.	Thermal desorption aerosol GC/MS (TAG), CPC bank including nano-water CPC	■		Iida et al. 2008; Kreisberg et al. 2009; Williams et al. 2010a; Williams et al. 2010b	US DOE DE-GF-02-05ER63997 NSF ATM-0506674 CARB 04-03
Hopke	Clarkson University	$PM_{2.5}$ filter sampling	■		Reemtsma et al. 2006	US EPA STAR R827354, RD832415
Jimenez	University of Colorado-Boulder	HR-ToF-AMS, C-ToF-AMS, Thermal denuder, SMPS, Cloud condensation nuclei counter, Grimm OPC Aerosol particle mass analyzer (APM)	■	■	DeCarlo et al. 2006; Zhang et al. 2007; Docherty et al. 2008; Cubison et al. 2008; Jimenez et al. 2009; Huffman et al. 2009a; Huffman et al. 2009b; Heald et al. 2010; Ng et al. 2010; Ervens et al. 2010; Farmer et al. 2010; Docherty et al., this paper	US EPA STAR RD-83216101-0, R831080 NSF ATM-0449815 NSF/UCAR S05-39607 NOAA NA08OAR4310565
Paulson	University of California - Los Angeles	Filter sampling, HPLC-flourosence peroxide analysis	■		Wang et al. 2010	CARB 04-319
Prather	University of California-San Diego	Aerosol Time-of-Flight Mass Spectrometer (ATOFMS), Ultrafine ATOFMS, Aircraft ATOFMS, SMPS Aerosol particle sizer (APS)	■	■	Spencer and Prather, 2006; Spencer et al. 2007; Denkenberger et al. 2007; Shields et al. 2008; Moffet et al. 2008; Pratt and Prather 2009 Pratt et al. 2009a; Pratt et al. 2009b Gaston et al 2010	NSF ATM-0321362, ATM-05011803, ATM-0528227 CARB 04-336 US EPA PM Center R827354
Schauer	University of Wisconsin-Madison	Standard Sunset semi-continuous EC/OC analyzer, 7-channel aethelometer, Hg speciation sampler, $PM_{2.5}$ filter sampling	■		Snyder et al. 2007; Snyder et al. 2008; Stone et al. 2009a; Stone et al. 2009b; Docherty et al. 2008; Sheelsey et al. 2010 Docherty et al., this paper	US EPA STAR R831080, RD-83216101-0, R-829798 NSF ATM-0449815
Seinfeld	California Institute of Technology	C-ToF-AMS, PILS-IC at Caltech (Pasadena)	■		Docherty et al. 2008	
Sioutas	University of Southern California	Ultrafine aerosol concentrator Aerosol particle mass analyzer (APM)	■		Geller et al. 2006; DeCarlo et al. 2006	US EPA STAR 53-4507-0482, 53-4507-7721
Thiemens	University of California-San Diego	Sulfate and nitrate isotope analysis	■			
Weber	Georgia Institute of Technology	PILS-WSOC, PILS-OC	■		Peltier et al. 2007; Docherty et al. 2008	CARB 98-316, EPA STAR RD-83216101-0
Worsnop	Aerodyne Research Inc.	HR-ToF-AMS, C-ToF-AMS with soft ionization	■			US DOE DE-FG02-04ER83890
Ziemann	University of California-Riverside	Thermal desorption particle beam mass spectrometer NO_x analyzer	■	■	Docherty et al., this paper	

414

Table S2. Average $TEOM_{FDMS}$, HR-AMS+EC, and $TEOM_{50C}$ final particle mass concentrations during SOAR-1 periods 1 (P1) and 2 (P2)

Measurement	P1 (7/18-8/1) Avg. ($\mu g\ m^{-3}$)	+/- S.D. ($\mu g\ m^{-3}$)	P2 (8/2-8/14) Avg. ($\mu g\ m^{-3}$)	+/- S.D. ($\mu g\ m^{-3}$)	P1 (7/18-8/1) ratio[a] ($\mu g\ m^{-3}$)	+/- S.D. ($\mu g\ m^{-3}$)	P2 (8/2-8/14) ratio[a] ($\mu g\ m^{-3}$)	+/- S.D. ($\mu g\ m^{-3}$)
$TEOM_{FDMS}$	26.36	10.89	31.79	11.4	na	na	na	na
HR-AMS+EC	18.29	7.98	24.36	10.46	0.69	0.6	0.77	0.56
$TEOM_{50C}$	15.87	6.55	13.96	4.88	0.6	0.58	0.44	0.5

[a] Ratio of measurement to $TEOM_{FDMS}$ mass (e.g., $x/TEOM_{FDMS}$)

Table S3. Statistical comparison of OC measurements by HR-AMS and Sunset instruments

	HR-AMS	Sunset 1	Sunset 2	Sunset 2 (+ SVOC)
Average (μgC m^{-3})	5.61	5.13	5.16	7.60
n	531	652	556	556
Absolute Difference[a]				
HR-AMS				
Sunset 1	1.09			
Sunset 2	1.28	1.04		
Sunset 2 (+ SVOC)	2.36	2.71	2.44	
Relative Difference[b]				
HR-AMS		0.21	0.25	0.31
Sunset 1	0.19		0.20	0.35
Sunset 2	0.23	0.20		0.32
Sunset 2 (+ SVOC)	0.42	0.53	0.47	
Relative Difference[c]				
HR-AMS		0.21	0.30	0.31
Sunset 1	0.20		0.23	0.34
Sunset 2	0.25	0.22		0.33
Sunset 2 (+ SVOC)	0.53	0.58	0.55	
r^2				
HR-AMS				
Sunset 1	0.53			
Sunset 2	0.36	0.42		
Sunset 2 (+ SVOC)	0.45	0.52	0.84	
Uncentered r^2				
HR-AMS				
Sunset 1	0.73			
Sunset 2	0.53	0.64		
Sunset 2 (+ SVOC)	0.54	0.66	0.98	

[a] Global average of absolute difference between measurements (e.g., avg[abs(row$_i$-column$_i$)])

[b] Absolute difference normalized by column global average (e.g., avg[abs(row$_i$-column$_i$)]/avg(column$_i$))

[c] Average value of individual relative absolute difference (e.g., avg[abs(row$_i$-column$_i$)/column$_i$])

Table S4. Results of linear regression and Pearson coefficients of correlation obtained from comparing MV-OOA components with select secondary tracer species.

			WSOC				O_x				Phthalic acid		
Component	Time block	Fig. 12	*N*	f(x) =	*r*	Fig. 12	*N*	f(x) =	*r*	Fig. 12	*N*	f(x) =	*r*
MV-OOA-hv	1800-0600	A	1016	0.49*x - 0.39	**0.52**	B	132	23.32*x -0.47	**0.54**	C	25	0.33*x - 0.38	**0.54**
	0600-1800	A	726	0.32*x + 0.04	**0.62**	B	198	22.02*x - 0.44	**0.50**	C	53	0.19*x - 0.44	0.42
	24-hour		1742		**0.75**		330		**0.71**		78	NA	**0.64**
MV-OOA-lv	1800-0600	D	1016	0.70*x - 0.41	0.47	E	132	24.9*x -0.50	0.06	F	25	0.15*x + 0.52	0.07
	0600-1800	D	726	0.76*x - 0.25	**0.64**	E	198	30.9*x - 0.62	0.25	F	53	0.34*x + 0.16	**0.81**
	24-hour		1742		**0.78**		330		**0.56**		78	NA	**0.81**
MV-OOA	1800-0600	G	1016	1.17*x - 0.78	**0.67**	H	132	60.2*x - 1.20	0.43	I	25	0.46*x + 0.49	0.43
	0600-1800	G	726	1.11*x - 0.28	**0.73**	H	198	58.0*x - 1.16	0.42	I	53	0.54*x + 0.57	**0.72**
	24-hour		1742		**0.86**		330		**0.72**		78	NA	**0.83**

Table S5. Average concentration of NR-PM_1 components and composition of HR-AMS+EC

Species	Concentration Avg. ($\mu g\ m^{-3}$)	Concentration S.D. ($\mu g\ m^{-3}$)	Mass fraction of HR-AMS+EC (%)
7/18-8/13-2005			
OA	9.12	3.59	44.40
EC	0.89	0.74	4.33
NH_4	2.48	1.38	12.07
NO_3	4.42	4.55	21.52
SO_4	3.55	1.09	17.28
Cl	0.09	0.08	0.44
HR-AMS+EC	20.54	9.42	
7/18-8/1/2005 (P1)			
OA	8.90	3.53	48.66
EC	0.99	0.81	5.41
NH_4	2.03	1.01	11.10
NO_3	2.93	3.03	16.02
SO_4	3.37	1.02	18.43
Cl	0.07	0.07	0.38
HR-AMS+EC	18.29	7.98	
8/2-8/13/2005 (P2)			
OA	9.50	3.67	44.48
EC	0.70	0.56	3.28
NH_4	3.25	1.56	15.22
NO_3	6.94	5.47	32.49
SO_4	3.85	1.15	18.02
Cl	0.11	0.09	0.51
HR-AMS+EC	21.36	10.46	

List of Abbreviations (in alphabetical order)

A-ATOFMS - aircraft aerosol time-of-flight mass spectrometer
AMS-PMF – PMF analysis of HR-AMS dataset
AMS – aerosol mass spectrometer
BAM - beta-attenuation monitor
BBOA - biomass burning OA
C-AMS – compact aerosol mass spectrometer
CE - collection efficiency
Cl – chloride
cLV-OOA – composite low-volatility OOA component
CMB-OMM – chemical mass balance of organic molecular markers
CO - carbon monoxide
d_a – aerodynamic diameter
d_{va} – vacuum aerodynamic diameter
EA – elemental analysis
EC – elemental carbon
f_{44} - ratio of unit resolution *m/z* 44 to total OA signal
GC/MS – gas chromatography/mass spectrometry
H/C – hydrogen:carbon ratio obtained from elemental analysis
HOA - hydrocarbon-like OA
HR – high resolution
HR-AMS – high Resolution aerosol mass spectrometer
HR-AMS+EC - the sum of HR-AMS NR-PM_1 and Sunset1 EC
HULIS - terrestrial humic-like substances
IC-nitrate - inorganic nitrate monitor
IC-sulfate – inorganic sulfate monitor
LOA – local OA component(s)
LOA-AC – amine-containing LOA component
LOA-2 – oxidized LOA component
MS - mass spectra
MV-OOA – medium-volatility OOA component
MV-OOA-lv – MV-OOA with relatively lower volatility
MV-OOA-hv - MV-OOA with relatively higher volatility
N/C – nitrogen:carbon ratio obtained from elemental analysis
NH_4 – ammonium
NH_4NO_3 - ammonium nitrate
NO_x - oxides of nitrogen
NO_3 – nitrate
NR-PM_1 – non-refractory submicron aerosol
NR-$PM_{2.5\text{-}1}$ - non-refractory material between $PM_{2.5}$ and PM_1
OA – organic aerosol
OC – organic carbon
O/C – oxygen:carbon ratio obtained from elemental analysis
OMM – organic molecular markers
OM/OC - organic mass:organic carbon ratio obtained from elemental analysis
ON – organonitrates
OOA - oxidized OA
OOC – oxidized organic carbon
OS – organosulfates
O_x - odd oxygen

O_3 - ozone
PILS-OC - particle-into-liquid sampler for total organic carbon
PM_f – fine particulate matter typically defined as particles having aerodynamic
PMF - positive matrix factorization
POA – primary OA
PST - Pacific Standard Time
Q-AMS - quadrupole AMS
RH - relative humidity
RIE - relative ionization efficiency
S/C – sulfur:carbon ratio obtained from elemental analysis
SOA – secondary organic aerosol
SOAR – Study of Organic Aerosols at Riverside
SOAR-1 – Study of Organic Aerosols at Riverside summer sampling period (July 15-August 15)
SOAR-2 - Study of Organic Aerosols at Riverside fall sampling period (date range)
diameters, d_a, $\leq$2.5 μm ($PM_{2.5}$) or $\leq$1 μm (PM_1))
SoCAB – South Coast Air Basin
SO_4 – sulfate
Sunset1 - standard Sunset semi-continuous OC/EC monitor
Sunset2 – dual-oven Sunset semi-continuous OC/EC monitor
SVM - semi-volatile material
SVOC – semi-volatile OC
SV-OOA – semi-volatile OOA
SVOM – semi-volatile organic material
TAG – thermal desorption aerosol gas chromatograph
TD – thermodenuder
TD-A-ATOFMS – A-ATOFMS interfaced with thermodenuder
TD-AMS – HR-AMS interfaced with thermodenuder
TD-AMS-PMF – PMF analysis of TD-AMS dataset
TEOM – tapered element oscillating microbalance
$TEOM_{50C}$ – heated (50°C) tapered element oscillating microbalance
$TEOM_{50C}$+NH_4NO_3 – $TEOM_{50C}$ supplemented with calculated NH_4NO_3 concentrations
$TEOM_{FDMS}$ – filter dynamics measurement system TEOM
ToF-AMS – time-of-flight aerosol mass spectrometer
UC-Riverside - University of California-Riverside
WSOC - water soluble organic carbon
UMR – unit mass resolution

Aiken, A. C., Decarlo, P. F., Kroll, J. H., Worsnop, D. R., Huffman, J. A., Docherty, K. S., Ulbrich, I. M., Mohr, C., Kimmel, J. R., Sueper, D., Sun, Y., Zhang, Q., Trimborn, A., Northway, M., Ziemann, P. J., Canagaratna, M. R., Onasch, T. B., Alfarra, M. R., Prevot, A. S. H., Dommen, J., Duplissy, J., Metzger, A., Baltensperger, U., and Jimenez, J. L.: O/C and OM/OC ratios of primary, secondary, and ambient organic aerosols with high-resolution time-of-flight aerosol mass spectrometry, Environmental Science & Technology, 42, 4478-4485, 10.1021/es703009q, 2008.

Aiken, A. C., Salcedo, D., Cubison, M. J., Huffman, J. A., DeCarlo, P. F., Ulbrich, I. M., Docherty, K. S., Sueper, D., Kimmel, J. R., Worsnop, D. R., Trimborn, A., Northway, M., Stone, E. A., Schauer, J. J., Volkamer, R. M., Fortner, E., de Foy, B., Wang, J., Laskin, A., Shutthanandan, V., Zheng, J., Zhang, R., Gaffney, J., Marley, N. A., Paredes-Miranda, G., Arnott, W. P., Molina, L. T., Sosa, G., and Jimenez, J. L.: Mexico City aerosol analysis during MILAGRO using high resolution aerosol mass spectrometry at the urban supersite (T0) - Part 1: Fine particle composition and organic source apportionment, Atmos. Chem. Phys., 9, 6633-6653, 2009.

Ban-Weiss, G. A., McLaughlin, J. P., Harley, R. A., M.M., L., Kirchsterrer, T. W., Kean, A. J., Strawa, A. W., Stevenson, E. D., and Kendall, G. R.: Long-term changes in emissions of nitrogen oxides and particulate matter from on-road gasoline and diesel vehicles, Atmospheric Environment, 2008.

Engel-Cox, J. A., and Weber, S. A.: Compilation and assessment of recent positive matrix factorization and UNMIX receptor model studies on fine particulate matter source apportionment for the eastern United States, J. Air Waste Manage. Assoc., 57, 1307-1316, 2007.

Erupe, M. E., Price, D. J., Silva, P. J., Malloy, Q. G. J., Qi, L., Warren, B., and Cocker III, D. R.: Secondary organic aerosol formation from reaction of tertiary amines with nitrate radical, Atmos. Chem. Phys. Discuss., 8, 16585-16608, 2008.
Herndon, S. C., author, S., author, T., and author, F.: The correlation of secondary organic aerosol with odd oxygen in a megacity outflow, Geophys. Res. Lett., 2007.

Gaston, C. J., Pratt, K. A., Qin, X. Y., and Prather, K. A.: Real-time detection and mixing state of methansulfonate in single particles at an inland urban location during a phytoplankton bloom, Environ. Sci. Technol., 44, 1566-1572, 2010.

Huffman, J. A., Docherty, K. S., Aiken, A. C., Cubison, M. J., Ulbrich, I. M., DeCarlo, P. F., Sueper, D., Jayne, J. T., Worsnop, D. R., Ziemann, P. J., and Jimenez, J. L.: Chemically-resolved aerosol volatility measurements from two megacity field studies, Atmos. Chem. Phys., 9, 7161-7182, 2009.

Ng, N. L., Canagaratna, M. R., Zhang, Q., Jimenez, J. L., Tian, J., Ulbrich, I. M., Kroll, J. H., Docherty, K. S., Chhabra, P. S., Bahreini, R., Murphy, S. M., Seinfeld, J. H., Hildebrandt, L., Donahue, N. M., DeCarlo, P. F., Lanz, V. A., Prevot, A. S. H., Dinar, E., Rudich, Y., and Worsnop, D. R.: Organic aerosol components observed in Northern Hemispheric datasets from Aerosol Mass Spectrometry, Atmos. Chem. Phys., 10, 4625-4641, 10.5194/acp-10-4625-2010, 2010.

Ng, N L., Canagaratna, M. R., Jimenez, J. L., Chhabra, P. S., Seinfeld, J. H., Worsnop, D. R.: Changes in organic aerosol composition with aging inferred from aerosol mass spectra, Atmos. Chem. Phys. Discuss., 11, 7095-7112, 2011.

Reff, A., Eberly, S. I., and Bhave, P. V.: Receptor modeling of ambient particulate matter data using positive matrix factorization: Review of existing methods, J. Air Waste Manage. Assoc., 57, 146-154, 2007.

Spracklen, D. V., Jimenez, J. L., Carslaw, K. S., Worsnop, D. R., Evans, M. J., Mass, G. W., Zhang, Q., Canagaratna, M. R., Allan, J., Coe, H., McFiggans, G., Rap, A., Forster, P.: Aerosol mass spectrometer constraint on the global secondary organic aerosol budget, Atmos. Chem. Phys. Discuss., 11, 5699-5755, 2011

Ulbrich, I. M., Canagaratna, M. R., Zhang, Q., Worsnop, D. R., and Jimenez, J. L.: Interpretation of organic components from Positive Matrix Factorization of aerosol mass spectrometric data, Atmos. Chem. Phys., 9, 2891-2918, 2009.

Zhang, Q., Worsnop, D. R., Canagaratna, M. R., and Jimenez, J. L.: Hydrocarbon-like and oxygenated organic aerosols in Pittsburgh: insights into sources and processes of organic aerosols, Atmos. Chem. Phys., 5, 3289-3311, 2005.